

SMART-3D: Three-Dimensional Self-Morphing Adaptive Replanning Tree

Priyanshu Agrawal[†] Shalabh Gupta^{†*} Zongyuan Shen[‡]

Abstract—This paper presents SMART-3D, an extension of the SMART algorithm to 3D environments. SMART-3D is a tree-based adaptive replanning algorithm for dynamic environments with fast moving obstacles. SMART-3D morphs the underlying tree to find a new path in real-time whenever the current path is blocked by obstacles. SMART-3D removed the grid decomposition requirement of the SMART algorithm by replacing the concept of hot-spots with that of hot-nodes, thus making it computationally efficient and scalable to 3D environments. The hot-nodes are nodes which allow for efficient reconnections to morph the existing tree to find a new safe and reliable path. The performance of SMART-3D is evaluated by extensive simulations in 2D and 3D environments populated with randomly moving dynamic obstacles. The results show that SMART-3D achieves high success rates and low replanning times, thus highlighting its suitability for real-time onboard applications.

Keywords: Path replanning; Dynamic environments; Autonomous robots; Adaptive navigation.

I. INTRODUCTION

Recent decades have seen significant growth of autonomous robots in supporting a diverse range of human operations. For example, unmanned underwater vehicles (UUVs) are used in different applications such as marine life exploration [1] [2], underwater terrain mapping [3]–[7], oceanic data measurement (e.g., salinity) [8], biological sampling [9], oil spill cleaning [10], [11], object recognition [12], diver action recognition [13], exploring mineral resources [14], target tracking [15]–[17], mine hunting [18], [19], energy-constrained sorties [20] and structural inspection [21]. Similarly, unmanned air vehicles (UAVs) are used in different applications such as environmental monitoring [22], surveillance [23], terrain mapping [24], tree inspection [25], smart agriculture [26] and bridge monitoring [27]. Most applications of autonomous robots consist of complex dynamic environments characterized by static as well as dynamic obstacles, where safe and reliable navigation becomes challenging. Fig. 1 shows an illustrative example, where a UAV is navigating in a city environment with buildings and other dynamic obstacles.

A. Motivation

In order for the autonomous robots to operate effectively in human-centric real-world environments, they need to be able to react and adapt their paths [28] in real-time to accommodate



Fig. 1. UAV flying in a city with both static and dynamic obstacles[#].

the changes in the environment. The standard path planning algorithms work offline to find an obstacle-free path that minimizes a given cost function, such as travel time. However, in dynamic environments, the robots require the ability to continuously replan in real-time due to moving obstacles. In addition to low travel times, these robots need to achieve low replanning times and high success rates (i.e., low probability of collision) [29] for safe and reliable navigation.

B. Literature Review

There are two types of strategies for planning in dynamic environments: active and reactive. Active planning strategies predict future obstacle trajectories to inform their plans. However, trajectory predictions specially for multiple obstacles could become computationally expensive and inaccurate [16], thus leading to unreliable paths. As such, reactive strategies have become popular, which use only current information of the environment and react to changes as they occur.

Technical literature consists of several tree-based replanning methods considering dynamic obstacles. These methods utilize different tree pruning and repair strategies to adapt the tree to dynamic obstacles and generate a new path. Such methods include Extended RRT (ERRT) [30], Dynamic RRT (DRRT) [31], Multipartite RRT (MPRRT) [32], RRT^X [33], Horizon-based Lazy RRT* (HLRRT*) [34], Efficient Bias-goal Factor RRT (EBGRRRT) [35] and Multi-objective Dynamic RRT*

[†] Dept. of Electrical and Computer Engineering, University of Connecticut, Storrs, CT, USA.

[‡] Robotics Institute, Carnegie Mellon University, Pittsburgh, PA, USA.

*Corresponding author (email: shalabh.gupta@uconn.edu)

[#] Image generated by ChatGPT

(MODRRT*) [36]. There also exist search-based methods, such as D* Lite [37] and Lifelong planning A* [38]. Some methods also incorporated steady [39] and spatio-temporally varying [40] currents for adaptive planning.

A recently proposed algorithm, called Self-Morphing Adaptive Replanning Tree (SMART) [29], performs fast reactive replanning for mobile robots in dynamic obstacle environments. A key distinct feature of SMART from the above tree-based methods is that it restricts the path feasibility check and tree-pruning to the robot's local neighborhood. Furthermore, SMART preserves the maximal tree structure via saving the multiple disjoint subtrees created after pruning infeasible colliding nodes and edges. These subtrees are then incrementally repaired and merged to form a morphed tree, which can produce the new collision-free path. The repair is done at hot-spots which are grid cells whose neighbors contain nodes of multiple-disjoint subtrees, thus providing avenues for easily reconnecting disjoint subtrees and perform repair. In rapidly changing environments, the algorithm outperformed the above tree-based and search-based reactive replanning algorithms in terms of travel time, success rate and replanning time [29]. A variant of SMART, called SMART-OC [41], adapted SMART to perform real-time time-risk optimal [42] replanning in response to dynamic obstacles and currents.

C. Contributions

SMART was developed for 2-dimensional environments, such as unmanned ground vehicles (UGVs) (e.g., wheel-base robots transporting goods in a factory) or unmanned surface vehicles (USVs) (e.g., autonomous boats operating offshore on an ocean surface). In this regard, this paper develops an extended version of SMART, called SMART-3D, which allows its deployment to robots (e.g., UAVs and UUVs) that operate in 3-dimensional environments. To facilitate computationally efficient operation in 3-D environments, SMART-3D replaced the concept of hot-spots that rely on grid decomposition for searching, with an equivalent concept of hot-nodes.

II. SMART-3D ALGORITHM

This section first presents a brief summary of the SMART-3D algorithm and then describes the necessary details. The main steps of SMART-3D are aligned with the steps of SMART [29]. Initially, SMART-3D constructs a planning tree using the RRT* algorithm considering only the static obstacles. This tree is then used to compute the initial path of the robot. While navigating, the robot constantly checks if its path is blocked by nearby dynamic obstacles. If the path is blocked, SMART-3D prunes the risky nodes in the local neighborhood of the robot. This breaks the RRT* tree and could result in the formation of multiple disjoint subtrees.

After pruning, SMART-3D performs the tree-repair to form a morphed tree, which can produce a new collision-free path. For tree-repair, it searches around the robot for critical nodes, called hot-nodes, whose neighboring nodes belong to atleast one other disjoint subtree. Then, the hot-nodes are ranked according to a distance-based utility heuristic. Next, the hot-nodes are incrementally selected based on their utility and

connected to their neighbors in different subtrees, thus merging the disjoint subtrees until a new path is found to the goal. This replanning process is repeated every time the robot's path is blocked by nearby dynamic obstacles until the goal is reached. SMART-3D is computationally very efficient because it performs path feasibility checking, tree-pruning, and hot-spot searching in the local vicinity of the robot and it utilizes the maximum disjoint tree-structure after pruning for quick tree-repair, thus producing a new path in real-time.

As compared to SMART [29], a key difference in SMART-3D is the removal of the grid decomposition of the space. SMART uses the grid decomposition to define and search for hot-spots. However, a grid-based search could become computationally expensive in 3D and higher dimensional spaces. As such, SMART-3D replaces the hot-spots with a functionally equivalent concept of hot-nodes, which are formally defined later. Thus, SMART-3D can be applied to higher dimensional spaces. While this paper focuses specifically on \mathbb{R}^3 space, it could be extended to \mathbb{R}^n spaces in general.

Now we present the details of the algorithm. Let $\mathcal{X} \subset \mathbb{R}^3$ be a space containing static and dynamic obstacles. Let $\mathcal{X}_N \subset \mathcal{X}$ be the configuration space free of static obstacles. Let $\mathcal{O} = \{O_i : i = 1, 2, \dots, m\}$ be the set of m dynamic obstacles. For ease and efficiency of collision checking, we assume that all obstacles are spherical, where $r_i \in \mathbb{R}^+$ is the radius of obstacle $O_i \in \mathcal{O}$. The position and speed of O_i at time $t \in \mathbb{R}^+$ are denoted by $x_i(t) \in \mathcal{X}_N$ and $v_i(t) \in \mathbb{R}^+$, respectively. Let R be a spherical robot of radius $r_R \in \mathbb{R}^+$, whose position and speed at time t are denoted by $x_R(t) \in \mathcal{X}_N$ and $v_R(t) \in \mathbb{R}^+$, respectively. Let (x_s, x_g) denote the start and goal positions.

A. Initialization

To initialize, a RRT* [43] tree $\mathcal{T}^0 \equiv (\mathcal{N}^0, \mathcal{E}^0)$ is constructed by considering only the static obstacles in the environment, where $(\mathcal{N}^0, \mathcal{E}^0)$ denote the pair of its node and edge sets. \mathcal{T}^0 is rooted at the goal x_g . In order to achieve the best replanning performance, \mathcal{T}^0 should cover \mathcal{X}_N with sufficient density such that new optimal paths could be found with ease without the need for further sampling and expanding the tree. Each node in the tree maintains a data structure containing information about its a) position, b) parent node, c) children nodes, d) subtree index, e) cost-to-go to the root, and f) status as active or pruned. Initially, all nodes are active and have the same index. An initial path σ^0 is found in \mathcal{X}_N using \mathcal{T}^0 .

B. Tree-Pruning

As the robot moves, σ^0 could be blocked by dynamic obstacles and become infeasible. Thus, in order to replan and find a safe path, it is required to prune the nodes and edges which are risky or colliding with these obstacles. To save computation effort and since the obstacles far away from the robot do not pose an immediate collision risk, the path feasibility checking and tree-pruning are done in a local neighborhood of the robot. This process is described below.

First, we define a Local Reaction Zone (LRZ) around the robot and an Obstacle Hazard Zone (OHZ) around each dynamic obstacle. While for 2D case the LRZ and OHZs are

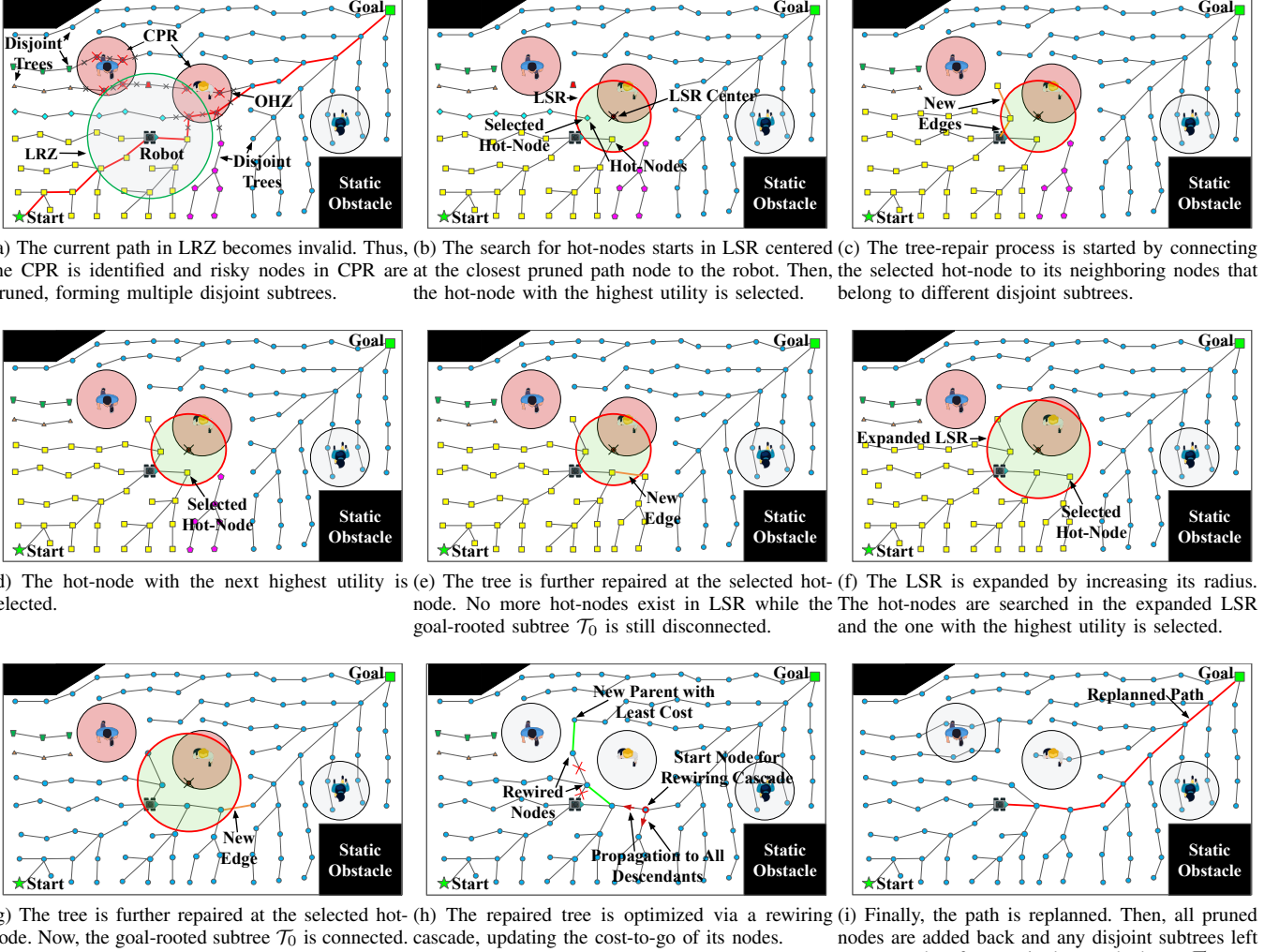


Fig. 2. Illustration of replanning done by SMART-3D: a) tree-pruning and disjoint subtree creation, and b)-i) tree-repair and replanning.

circular disks, for 3D case they are spheres centered at the robot. The LRZ represents the region reachable by the robot in a certain reaction time-horizon. The OHZ is a high-risk region around a given obstacle. Since obstacles could have unpredictable movements, the OHZ is defined as a sphere with the obstacle's radius plus its speed times a risk time-horizon. The LRZ and OHZ are defined [29] as follows:

Definition II.1 (LRZ). *The LRZ for a robot \mathcal{R} is defined as $LRZ_{\mathcal{R}}(t) = \{x \in \mathcal{X}_N : \|x - x_{\mathcal{R}}(t)\| \leq v_{\mathcal{R}}(t) \times T_{RH}\}$, where $T_{RH} \in \mathbb{R}^+$ is the robot reaction time-horizon.*

Definition II.2 (OHZ). *The OHZ for an obstacle $O_i \in \mathcal{O}$ is defined as $OHZ_i(t) = \{x \in \mathcal{X}_N : \|x - x_i(t)\| \leq v_i(t) \times T_{OH} + r_i + r_{\mathcal{R}}\}$, where $T_{OH} \in \mathbb{R}^+$ is the obstacle risk time-horizon.*

Note: For convenience, the robot radius $r_{\mathcal{R}}$ is added to the OHZ to then treat the robot as a point size.

The nearby obstacles whose OHZs intersect with the robot's LRZ at a certain time can pose a collision risk to the robot. Thus, the nodes and edges in these OHZs must be pruned as they cannot be used to plan a new path. The union of all these OHZs form a Critical Pruning Region (CPR) as defined below.

Definition II.3 (CPR). *Let \mathcal{D} denote all obstacles that are intersecting with the robot's LRZ and pose danger to the robot such that $\mathcal{D} = \{O_i \in \mathcal{O} : LRZ_{\mathcal{R}}(t) \cap OHZ_i(t) \neq \emptyset\}$. Then, the CPR is defined as*

$$CPR(t) = \bigcup_{\mathcal{D}} OHZ_i(t). \quad (1)$$

The robot constantly checks the feasibility of the portion of its current path in LRZ. If the current path in LRZ is invalid, then all nodes and edges that fall in the entire CPR are pruned. If a node falls in CPR, then it is pruned along with its connecting edges. If an edge falls in CPR although it is connected to two safe nodes outside CPR, then it is pruned but its end nodes are kept. Figure 2a shows an illustrative example of tree-pruning in CPR when the robot's current path in its LRZ is blocked by an obstacle. The tree-pruning process could result in creation of multiple disjoint subtrees.

Definition II.4 (Disjoint Subtree). *A disjoint subtree is a broken portion of the current tree \mathcal{T} whose root is either the goal or a child of a pruned node or edge.*

Let $\mathcal{T} \equiv (\mathcal{N}, \mathcal{E})$ be the current tree. Suppose the tree-pruning process breaks \mathcal{T} into $K \in \mathbb{N}^+$ different disjoint subtrees denoted by $\mathcal{T}_0, \mathcal{T}_1, \dots, \mathcal{T}_{K-1}$. Here $\mathcal{T}_0 \equiv (\mathcal{N}_0, \mathcal{E}_0)$ is the subtree rooted at the goal. Let $\mathcal{N}^a \in \mathcal{N}$ and $\mathcal{N}^p \in \mathcal{N}$ be the sets of all alive and pruned nodes, respectively, such that $\mathcal{N} = \mathcal{N}^a \cup \mathcal{N}^p$.

Each node $n \in \mathcal{N}^a$ stores its own subtree index. When a node is pruned, its children (none, one or many) become the roots of their own disjoint subtrees and the subtree indices are updated for all their descendants. Similarly, when an edge is pruned, the orphaned node becomes the root of its own disjoint subtree and the subtree index is updated for all its descendants.

C. Tree Repair

The objective of tree-repair is to stitch together all disjoint subtrees formed after the tree-pruning process to form a single morphed tree which can then be used to obtain a new path to the goal. Since the node density of \mathcal{T} is sufficiently high in the free space outside CPR, it's easy to repair the disjoint subtrees into a single tree by making simple reconnections. Thus, it is required to identify nodes which can be easily connected with nodes of other disjoint subtrees.

As compared to hot-spots [29] in SMART, this paper uses the concept of hot-nodes, which does not require a grid decomposition, thus making the algorithm computationally efficient and extendable to high-dimensional spaces. The tree-repair process works by searching for hot-nodes and incrementally making reconnections between disjoint subtrees at the hot-nodes with the highest utilities.

Definition II.5 (Neighbor). A node $n_j \in \mathcal{N}^a$ is said to be a neighbor of node $n_i \in \mathcal{N}^a$ if $x_{n_j} \in \mathcal{B}(x_{n_i}, r)$, where $x_{n_i} \in \mathcal{X}_N$ and $x_{n_j} \in \mathcal{X}_N$ are the positions of n_i and n_j , respectively, and $\mathcal{B}(x_{n_i}, r)$ is a ball of radius r centered at n_i .

Definition II.6 (Eligible Neighbor). A neighbor $n_j \in \mathcal{N}^a$ of node $n_i \in \mathcal{N}^a$ is said to be an eligible neighbor if it belongs to a different disjoint subtree than n_i and the nodes n_i and n_j could be connected by a feasible edge.

Definition II.7 (Hot-Node). A node $n \in \mathcal{N}^a$ is said to be a hot-node if it has at least one eligible neighbor.

1) *Search for Hot-Nodes*: The search for hot-nodes begins around the damaged path. Therefore, we define a Local Search Region (LSR) centered at the pruned node on the damaged path which is nearest to the robot.

Definition II.8 (LSR). Let $\hat{n} \in \mathcal{N}^p$ be the pruned path node closest to the robot. Let $x_{\hat{n}}$ be the location of \hat{n} . Let r_s be the search radius. Then, the LSR is defined as $\text{LSR}(r_s) = \{x \in \mathcal{X}_N : \|x - x_{\hat{n}}\| \leq r_s\}$.

At each replanning incident, the search radius r_s is initialized to be a user-specified radius, r_{s_0} . Then, the LSR is searched and all hot-nodes are identified. Fig. 2b shows an example of hot-node search in LSR. If there are no hot-nodes in LSR, then the LSR is expanded by multiplying r_s by an expansion factor $\lambda > 1$ (Fig. 2f). This process is repeated until at least one hot-node is found.

Algorithm 1: SMART-3D

```

1  $\{\mathcal{T}^0, \sigma^0\} \leftarrow \text{RRT}^*(x_s, x_g, \mathcal{X}_N)$ ; // initialization
2  $t = t_0$ ,  $\mathcal{T} = \mathcal{T}^0$ ,  $\sigma = \sigma^0$ ;
3 while  $x_{\mathcal{R}} \neq x_g$  do // goal unreached
4    $t \leftarrow \text{UpdateClock}()$ ;
5    $\{x_i(t), v_i(t)\}_{i=1..m} \leftarrow \text{UpdateObstacleState}()$ ;
6    $\{x_{\mathcal{R}}(t), v_{\mathcal{R}}(t)\} \leftarrow \text{UpdateRobotState}()$ ;
7   if  $\text{ValidatePath}(\sigma, \text{LRZ}_{\mathcal{R}}(t), \{\text{OHZ}_i(t)\}_{i=1..m})$  then
8      $\text{Navigate}(\sigma)$ ;
9   else
10     $\sigma \leftarrow \text{void}$ ; // invalid path
11     $\{\mathcal{T}_0, \dots, \mathcal{T}_{K-1}\} \leftarrow \text{TreePruning}(\mathcal{T}, \text{CPR}(t))$ ; // II-B
12     $r_s \leftarrow r_{s_0}$ ,  $\mathcal{H} \leftarrow \emptyset$ ,  $\mathcal{N}_s \leftarrow \emptyset$ ; // initialize repair
13    while  $\mathcal{T}_0$  is not reachable from  $x_{\mathcal{R}}$  do
14      if  $r_s < r_{s_{\max}}$  then // informed tree-repair
15         $r_s \leftarrow r_s \times \lambda$ ;
16         $\mathcal{H} \leftarrow \text{HotNodeSearch}(\text{LSR}(r_s))$ ; // II-C1
17         $\mathcal{U} \leftarrow \text{ComputeUtility}(\mathcal{H})$ ; // II-C2
18         $\{\mathcal{N}_s, \mathcal{T}_0\} \leftarrow \text{TreeReconnection}(\mathcal{H}, \mathcal{U})$ ;
19        // II-C3
20      else // standard tree-repair
21         $x_{rand} \leftarrow \text{SampleFree}()$ ;
22        Join  $x_{rand}$  to all nearby reachable subtrees;
23        if  $x_{rand} \in \mathcal{T}_0$  then  $\text{Rewire}(x_{rand})$ ;
24      end
25    end
26     $\mathcal{T}_0 \leftarrow \text{TreeOptimization}(\mathcal{T}_0, \mathcal{N}_s)$ ; // II-D
27     $\sigma \leftarrow \text{PathSearch}(x_{\mathcal{R}}, x_g, \mathcal{T}_0)$ ; // II-E
28    Add  $\mathcal{N}^p$  and disjoint subtrees to  $\mathcal{T}_0$  to get a single tree  $\mathcal{T}$ ;
29 end

```

2) *Ranking of Hot-Nodes*: After all hot-nodes are detected in the LSR, they are ranked by utility as defined as follows.

Definition II.9 (Utility). The utility of a hot-node n is computed as follows:

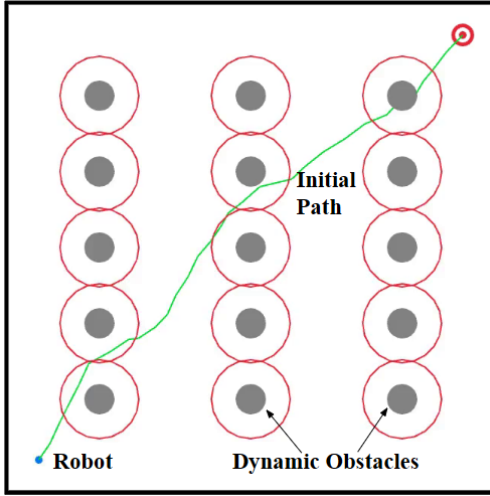
$$\mathcal{U}(n) = \begin{cases} \frac{1}{\|x_{\mathcal{R}} - x_n\|_2 + \|x_n - x_{n'}\|_2 + g(n')}, & \text{if } n' \in \mathcal{N}_0 \\ \frac{1}{\|x_{\mathcal{R}} - x_n\|_2 + \|x_n - x_{n'}\|_2 + \|x_{n'} - x_g\|_2}, & \text{if } n' \notin \mathcal{N}_0 \end{cases} \quad (2)$$

where n' is the nearest eligible neighbor of n ; x_n and $x_{n'}$ are the positions of n and n' , respectively; and $g(n')$ returns the travel cost from n' to the goal on \mathcal{T}_0 .

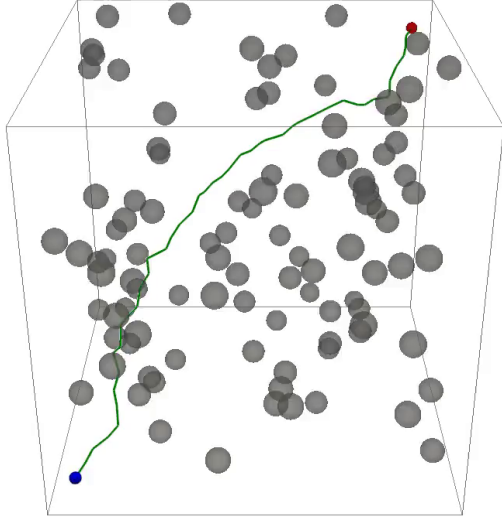
Thus, if the nearest neighbor n' of hot-node n belongs to the goal-rooted tree \mathcal{T}_0 , then the actual cost-to-go is used as the distance to the goal, otherwise a heuristic cost is used.

3) *Tree-reconnections*: Once the hot-nodes in LSR are identified and ranked, tree reconnections are done. This consists of the following steps:

- Pick the hot-node in LSR with the highest utility (Figs. 2b, 2d). If no hot-nodes are left in LSR, then go back to search in expanded LSR (Fig. 2f).
- Pick the nearest eligible neighbor of the hot-node and connect it (Figs. 2c, 2e, 2g).
- Update the parent-child relationships and subtree indices (Figs. 2c, 2e, 2g) as follows: 1) if any node from the above node-pair belongs to \mathcal{T}_0 , then this node is set as the parent and all nodes of the other connected subtree are assigned the index of \mathcal{T}_0 and their cost-to-go are updated, or 2) if none of the nodes in the above node-pair belongs to \mathcal{T}_0 , then one of them is set as the parent and all nodes of the other connected subtree are assigned its index.



(a) 2D Scenario with 15 dynamic obstacles. The initial path (green) connects the start (blue) and goal (red) points.



(b) 3D Scenario with 100 randomly distributed dynamic obstacles. The initial path (green) connects the start (blue) and goal (red) points.

Fig. 3. Examples of 2D and 3D scenarios. Initial path is found for both these scenarios using RRT* without considering dynamic obstacles.

TABLE I
PARAMETERS FOR 2D AND 3D SCENARIOS

Parameter	2D Scenario	3D Scenario
Risk Time-Horizon (T_{OH})	0.4 s	0.4 s
Reaction Time-Horizon (T_{RH})	1 s	1 s
LSR Initial Radius (r_{s_0})	1 m	1 m
LSR Expansion Factor (λ)	1.5	1.5
LSR Max Radius ($r_{s_{max}}$)	10 m	10 m
Neighborhood Radius (r)	1.7 m	1.7 m
Initial RRT* Steering Range	1 m	1 m
Initial RRT* Iterations	2500	20000

- d. Update the hot-nodes in LSR and their utilities.
- e. Check if \mathcal{T}_0 is reachable from x_R (Fig. 2g). If true, then a path can be found to the goal; otherwise return to step a above.

Note: If the entire space is exhausted by tree-repair and no path is found using alive samples, then random sampling and repairing is done for probabilistic completeness.

D. Tree-Optimization

During tree-repair, several subtrees were merged with \mathcal{T}_0 . These subtrees are optimized using a rewiring cascade starting from all subtree nodes \mathcal{N}_s connected to \mathcal{T}_0 (Fig. 2h).

E. Path Search

After the merged tree is optimized, an updated path σ is found using this tree (Fig. 2i). After we find a new path, all nodes in \mathcal{N}^p and the roots of the remaining disjoint subtrees are reconnected with \mathcal{T}_0 and a single tree \mathcal{T} is formed.

Algorithm 1 shows the workings of SMART-3D. The pseudocode remains the same as that of [29], with the exception that the hot-spot search is replaced with a hot-node search.

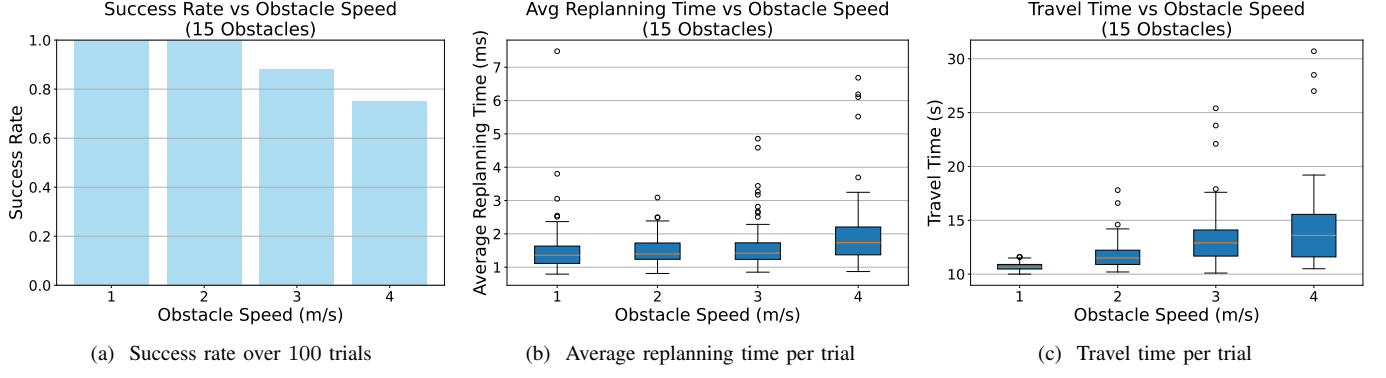
III. RESULTS

This section presents the performance results of SMART-3D via Monte carlo simulations of a robot traversing in open environments with several dynamic obstacles. The robot is considered to be holonomic with radius $r_R = 0.5\text{m}$ and speed $v_R = 4\text{m/s}$. For simplicity, we treat the robot as a point and add its radius to the OHZs for collision checking. The results are shown for 2D and 3D environments. Table I lists all parameters for the 2D and 3D simulations. Each simulation trial has a timestep of 0.1s . If any replanning event takes longer than 0.1s , the whole trial is marked as failed. However, this is rare and typically occurs in the case where multiple obstacles surround the robot such that there is no solution, or the only solution is through an extremely narrow opening between obstacles. Also, if a collision occurs, then the trial is marked as failed. For successful trials, the following performance metrics are used for validation:

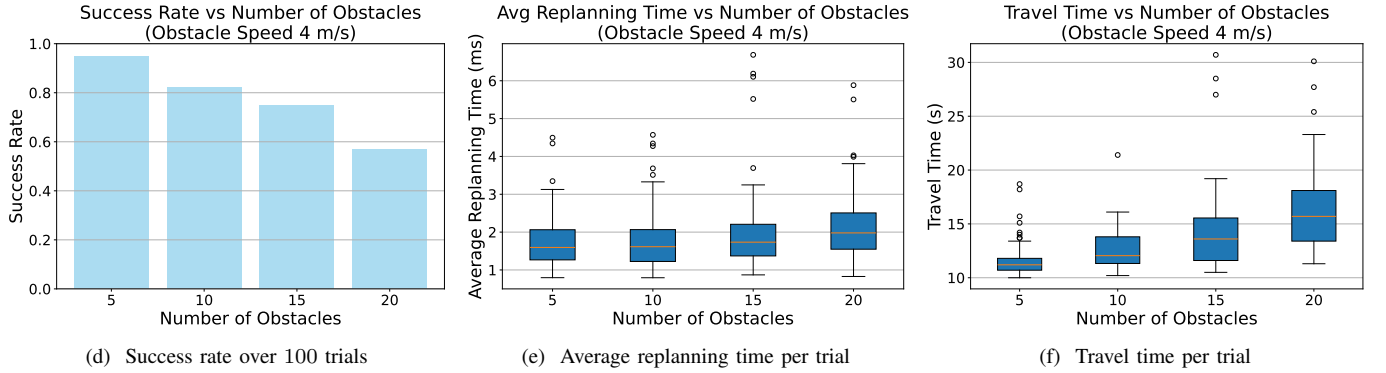
- *Replanning time*: Time taken by the robot to replan its path when its current path is broken.
- *Success rate*: Fraction of successful trials where the robot reached the goal without collision.
- *Travel time*: Time taken by the robot to travel from the start to the goal on a successful trial.

A. 2D Scenario

First, SMART-3D's performance is validated for a 2D scenario. Fig. 3a shows an example of a $32\text{m} \times 32\text{m}$ scenario with 15 dynamic obstacles. In this scenario, the start and goal points of the robot are located at $(2\text{m}, 2\text{m})$ and $(30\text{m}, 30\text{m})$, respectively. Each obstacle is considered to be circular with a radius of 0.5m . The obstacles continuously move in a random heading from $[0, 2\pi]$ for a random distance from $[0, 10]\text{m}$, after which a new heading and distance are selected. The obstacles are allowed to overlap during traveling.



2D Case 1: Number of obstacles is fixed to be 15 and obstacle speed is varied from 1m/s to 4m/s.



2D Case 2: Obstacle speed is fixed to be 4m/s and number of obstacles is varied from 5 to 20.

Fig. 4. Performance results of simulation experiments for the two case studies of the 2D scenario.

Two case studies are conducted as follows.

1) 2D Case 1: Number of obstacles fixed but speed varied:

In the first 2D case study, the number of dynamic obstacles is fixed to be 15, while the obstacle speed is varied. In any particular simulation trial, all obstacles move at the same constant speed chosen from the set $\{1, 2, 3, 4\}$ m/s. For each obstacle speed, we run 100 trials, where in each trial the obstacles move randomly as described above. Then, a different speed is chosen, and the trials are repeated. In this manner, the statistical performance is recorded for four different speeds.

2) 2D Case 2: Speed fixed but number of obstacles varied:

In the second 2D case study, the speed of obstacles is fixed to be 4m/s, while the number of dynamic obstacles is varied. In any particular simulation trial, the number of obstacles is chosen from the set $\{5, 10, 15, 20\}$. For each number of obstacles, we run 100 trials, where in each trial the obstacles move randomly as described above. Then, a different number of obstacles is chosen, and the trials are repeated. In this manner, the statistical performance is recorded for four different numbers of obstacles.

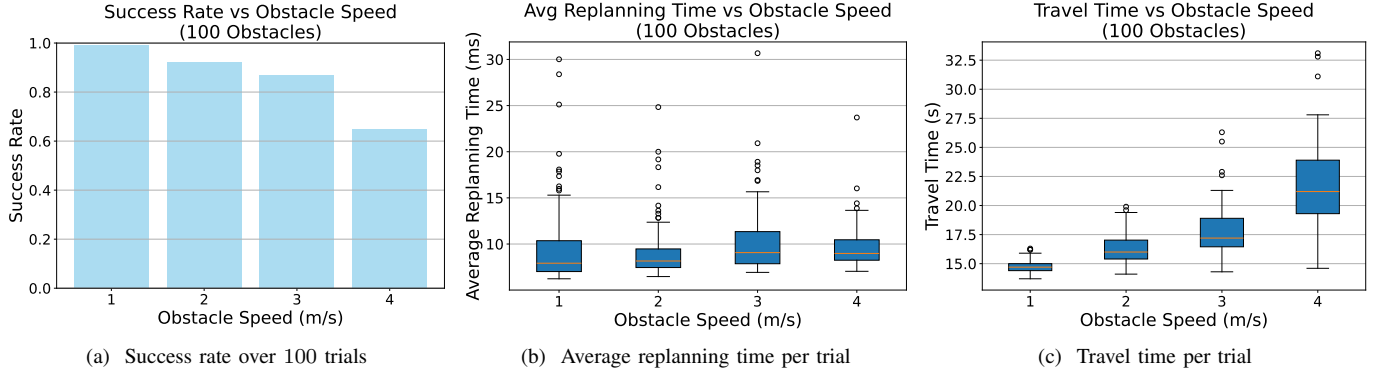
Fig. 4 shows the performance results for the two case studies of the 2D scenario. For case study 1, Figs 4a, 4b and 4c show the plots of success rate over 100 trials, average replanning time per trial and travel time per trial, respectively. The average replanning time is calculated over all replanning incidents in

any trial. The results show that SMART-3D achieves similar performance as that of SMART [29] for the 2D scenario. For obstacle speeds of 1, 2, 3 and 4m/s, SMART-3D achieves success rates of 1.0, 1.0, 0.88 and 0.75, respectively. The median of the average replanning time per trial falls between 1 to 2 milliseconds for every obstacle speed. The median travel times are approximately 10.7s, 11.5s, 12.9s and 13.6s, respectively. For case study 2, Figs 4d, 4e and 4f show the plots of success rate over 100 trials, average replanning time per trial, and travel time per trial, respectively. The success rate decreases as the number of obstacles is increased. The median of the average replanning time per trial falls between 1 to 2 milliseconds. The travel time increases with the number of obstacles due to more diversions and replannings.

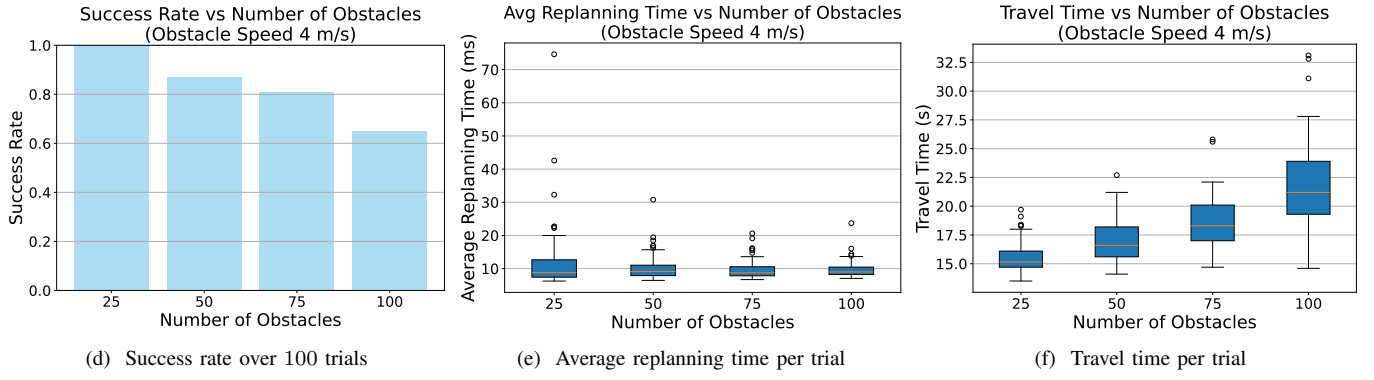
B. 3D Scenario

Next, SMART-3D's performance is validated for a 3D scenario. Fig. 3b shows an example of a $32m \times 32m \times 32m$ scenario with 100 dynamic obstacles. In this scenario, the start and goal points of the robot are located at (2m, 2m, 2m) and (30m, 30m, 30m), respectively. Each obstacle is considered to be sphere with a radius of 0.5m. The obstacles are initialized at random positions. They continuously move to randomly selected waypoints within the 3D space. The obstacles are allowed to overlap during traveling.

Two case studies are conducted as follows.



3D Case 1: Number of obstacles is fixed to be 100 and obstacle speed is varied from 1m/s to 4m/s.



3D Case 2: Obstacle speed is fixed to be 4m/s and number of obstacles is varied from 25 to 100.

Fig. 5. Performance results of simulation experiments for the two case studies of the 3D scenario.

1) 3D Case 1: Number of obstacles fixed but speed varied:

In the first 3D case study, the number of dynamic obstacles is fixed to be 100, while the obstacle speed is varied. In any particular simulation trial, all obstacles move at the same constant speed chosen from the set $\{1, 2, 3, 4\}$ m/s. For each obstacle speed, we run 100 trials, where in each trial the obstacles move randomly as described above. Then, a different speed is chosen, and the trials are repeated. In this manner, the statistical performance is recorded for four different speeds.

2) 3D Case 2: Speed fixed but number of obstacles varied:

In the second 3D case study, the speed of obstacles is fixed to be 4 m/s, while the number of dynamic obstacles is varied. In any particular simulation trial, the number of obstacles is chosen from the set $\{25, 50, 75, 100\}$. For each number of obstacles, we run 100 trials, where in each trial the obstacles move randomly as described above. Then, a different number of obstacles is chosen, and the trials are repeated. In this manner, the statistical performance is recorded for four different numbers of obstacles.

Fig. 5 shows the performance results for the two case studies of the 3D scenario. For case study 1, Figs 5a, 5b and 5c show the plots of success rate over 100 trials, average replanning time per trial and travel time per trial, respectively. Overall, SMART-3D achieves high success rates of around or above 90% for all obstacle speeds of 3 m/s or less. As expected, the success rate decreases as the obstacle speed is increased. The

median of the average replanning time per trial falls below 10 milliseconds for every obstacle speed, which is slightly higher than the 2D scenario but fast enough for real-time applications. The median travel time increases with the obstacle speed due to more diversions and replannings. For case study 2, Figs 5d, 5e and 5f show the plots of success rate over 100 trials, average replanning time per trial and travel time per trial, respectively. They show similar trends, where the success rate decreases with the number of obstacles, the median of the average replanning time stays below 10 milliseconds, and the travel time increases with the number of obstacles.

IV. CONCLUSION AND FUTURE WORK

This paper developed the SMART-3D algorithm which is an extension of the SMART algorithm [29] to 3D spaces. By removing the need for a grid decomposition and replacing hot-spots with hot-nodes, SMART-3D scales well to a 3D environment with computational efficiency. The results for both 2D and 3D scenarios demonstrated that SMART-3D achieves high success rates and low replanning times, thus making it suitable for real-time applications.

In future work, SMART-3D can be further extended to motion planning problems including time-risk optimization of non-holonomic robots [44], distributed multi-robot navigation [45], and object manipulation using robotics arms with complex configuration spaces.

APPENDIX

Code Availability

The code for SMART-3D is available at: <https://github.com/LinksLabUConn/SMART3D>.

REFERENCES

- [1] R. K. Katzschnmann, J. Del Preto, R. MacCurdy, and D. Rus, "Exploration of underwater life with an acoustically controlled soft robotic fish," *Science Robotics*, vol. 3, no. 16, 2018.
- [2] J. Yuh, G. Marani, and D. R. Blidberg, "Applications of marine robotic vehicles," *Intelligent Service Robotics*, vol. 4, no. 4, pp. 221–231, 2011.
- [3] Z. Shen, J. Song, K. Mittal, and S. Gupta, "CT-CPP: Coverage path planning for 3D terrain reconstruction using dynamic coverage trees," *IEEE Robot. Autom. Lett.*, vol. 7, no. 1, pp. 135–142, 2022.
- [4] Z. Shen, J. P. Wilson, and S. Gupta, "C*: A coverage path planning algorithm for unknown environments using rapidly covering graphs," 2025. [Online]. Available: <https://arxiv.org/abs/2505.13782>
- [5] N. Palomeras, N. Hurtós, M. Carreras, and P. Ridao, "Autonomous mapping of underwater 3-D structures: From view planning to execution," *IEEE Robot. Autom. Lett.*, vol. 3, no. 3, pp. 1965–1971, 2018.
- [6] J. Song and S. Gupta, " ϵ^* : An online coverage path planning algorithm," *IEEE Trans. Robot.*, vol. 34, no. 2, pp. 526–533, 2018.
- [7] S. Negahdaripour and H. Madjidi, "Stereovision imaging on submersible platforms for 3-D mapping of benthic habitats and sea-floor structures," *IEEE Journal of Oceanic Engineering*, vol. 28, no. 4, pp. 625–650, 2003.
- [8] T. Somers and G. A. Hollinger, "Human–robot planning and learning for marine data collection," *Autonomous Robots*, vol. 40, no. 7, p. 1123–1137, 2016.
- [9] K. C. Galloway, K. P. Becker, B. Phillips, J. Kirby, S. Licht, D. Tchernov, R. J. Wood, , and D. F. Gruber, "Soft robotic grippers for biological sampling on deep reefs," *Soft Robotics*, vol. 3, no. 1, pp. 23–33, 2016.
- [10] J. Song, S. Gupta, J. Hare, and S. Zhou, "Adaptive cleaning of oil spills by autonomous vehicles under partial information," in *Proc. OCEANS'13 MTS/IEEE*, San Diego, CA, USA, Sep. 2013, pp. 1–5.
- [11] S. V. Kumar, R. Jayaparthy, and B. Priyanka, "Efficient path planning of AUVs for container ship oil spill detection in coastal areas," *Ocean Engineering*, vol. 217, 2020.
- [12] G. L. Foresti and G. Stefania, "A hierarchical classification system for object recognition in underwater environments," *IEEE Journal of oceanic engineering*, vol. 27, no. 1, pp. 66–78, 2002.
- [13] J. Yang, J. P. Wilson, and S. Gupta, "Dare: Diver action recognition encoder for underwater human–robot interaction," *IEEE Access*, vol. 11, pp. 76 926–76 940, 2023.
- [14] N. Wakita, K. Hirokawa, T. Ichikawa, and Y. Yamauchi, "Development of autonomous underwater vehicle (AUV) for exploring deep sea marine mineral resources," *Mitsubishi Heavy Industries Technical Review*, vol. 47, no.3, pp. 73–80, 2010.
- [15] K. Shojaei and M. Dolatshahi, "Line-of-sight target tracking control of underactuated autonomous underwater vehicles," *Ocean Engineering*, vol. 133, pp. 244–252, 2017.
- [16] J. Z. Hare, S. Gupta, and T. A. Wettergren, "POSE.3C: Prediction-based opportunistic sensing using distributed classification, clustering and control in heterogeneous sensor networks," *IEEE Transactions on Control of Network Systems*, vol. 6, no. 4, pp. 1438–1450, 2019.
- [17] J. Z. Hare, J. Song, S. Gupta, and T. A. Wettergren, "POSE.R: Prediction-based opportunistic sensing for resilient and efficient sensor networks," *ACM Transactions on Sensor Networks*, vol. 17, no. 5, pp. 1–41, 2020.
- [18] E. U. Acar, H. Choset, Y. Zhang, and M. Schervish, "Path planning for robotic demining: Robust sensor-based coverage of unstructured environments and probabilistic methods," *The International Journal of Robotics Research*, vol. 22, no. 7-8, pp. 441–466, 2003.
- [19] K. Mukherjee, S. Gupta, A. Ray, and S. Phoha, "Symbolic analysis of sonar data for underwater target detection," *IEEE J. Oceanic Eng.*, vol. 36, no. 2, pp. 219–230, 2011.
- [20] Z. Shen, J. P. Wilson, and S. Gupta, " ϵ^*+ : An online coverage path planning algorithm for energy-constrained autonomous vehicles," in *Global Oceans 2020: Singapore – U.S. Gulf Coast*, 2020, pp. 1–6.
- [21] G. L. Foresti, "Visual inspection of sea bottom structures by an autonomous underwater vehicle," *IEEE Transactions on Systems, Man, and Cybernetics, Part B (Cybernetics)*, vol. 31, no. 5, pp. 691–705, 2001.
- [22] M. Dunbabin and L. Marques, "Robots for environmental monitoring: Significant advancements and applications," *IEEE Robotics & Automation Magazine*, vol. 19, no. 1, pp. 24–39, 2012.
- [23] K. Mukherjee, S. Gupta, A. Ray, and T. A. Wettergren, "Statistical-mechanics-inspired optimization of sensor field configuration for detection of mobile targets," *IEEE Transactions on Systems, Man, and Cybernetics, Part B (Cybernetics)*, vol. 41, no. 3, pp. 783–791, 2011.
- [24] F. O. Coelho, M. F. Pinto, I. Z. Biundini, G. G. R. Castro, F. A. A. Andrade, and A. L. M. Marcato, "Autonomous uav exploration and mapping in uncharted terrain through boundary-driven strategy," *IEEE Access*, vol. 12, pp. 92 464–92 483, 2024.
- [25] G. G. R. d. Castro, G. S. Berger, A. Cantieri, M. Teixeira, J. Lima, A. I. Pereira, and M. F. Pinto, "Adaptive path planning for fusing rapidly exploring random trees and deep reinforcement learning in an agriculture dynamic environment uavs," *Agriculture*, vol. 13, no. 2, 2023. [Online]. Available: <https://www.mdpi.com/2077-0472/13/2/354>
- [26] S. Moradi, A. Bokani, and J. Hassan, "Uav-based smart agriculture: a review of uav sensing and applications," in *2022 32nd International Telecommunication Networks and Applications Conference (ITNAC)*, 2022, pp. 181–184.
- [27] T. Panigati, M. Zini, D. Striccoli, P. F. Giordano, D. Tonelli, M. P. Limongelli, and D. Zonta, "Drone-based bridge inspections: Current practices and future directions," *Automation in Construction*, vol. 173, p. 106101, 2025. [Online]. Available: <https://www.sciencedirect.com/science/article/pii/S0926580525001414>
- [28] S. Gupta, A. Ray, and S. Phoha, "Generalized ising model for dynamic adaptation in autonomous systems," *Euro. Phys. Lett.*, vol. 87, p. 10009, 2009.
- [29] Z. Shen, J. P. Wilson, S. Gupta, and R. Harvey, "Smart: Self-morphing adaptive replanning tree," *IEEE Robotics and Automation Letters*, vol. 8, no. 11, pp. 7312–7319, 2023.
- [30] J. Bruce and M. Veloso, "Real-time randomized path planning for robot navigation," in *IEEE Int. Conf. Intell. Robots Syst.*, vol. 3, 2002, pp. 2383–2388.
- [31] D. Ferguson, N. Kalra, and A. Stentz, "Replanning with RRTs," in *IEEE Int. Conf. Robot. Automat.*, 2006, pp. 1243–1248.
- [32] M. Zucker, J. Kuffner, and M. Branicky, "Multipartite RRTs for rapid replanning in dynamic environments," in *IEEE Int. Conf. Robot. Automat.*, 2007, pp. 1603–1609.
- [33] M. Otte and E. Frazzoli, "RRT^X: Asymptotically optimal single-query sampling-based motion planning with quick replanning," *Int. J. Robot. Res.*, vol. 35, no. 7, pp. 797–822, 2016.
- [34] Y. Chen, Z. He, and S. Li, "Horizon-based lazy optimal RRT for fast, efficient replanning in dynamic environment," *Auton. Robots*, vol. 43, no. 8, pp. 2271–2292, 2019.
- [35] C. Yuan, G. Liu, W. Zhang, and X. Pan, "An efficient RRT cache method in dynamic environments for path planning," *Robot. Auton. Syst.*, vol. 131, p. 103595, 2020.
- [36] J. Qi, H. Yang, and H. Sun, "MOD-RRT*: A sampling-based algorithm for robot path planning in dynamic environment," *IEEE Trans. Ind. Electron.*, vol. 68, no. 8, pp. 7244–7251, Aug. 2021.
- [37] S. Koenig and M. Likhachev, "D* Lite," in *Eighteenth National Conference on Artificial Intelligence*. USA: American Association for Artificial Intelligence, 2002, p. 476–483.
- [38] S. Koenig, M. Likhachev, and D. Furcy, "Lifelong Planning A*," *Artificial Intelligence*, vol. 155, no. 1-2, pp. 93–146, 2004.
- [39] K. Mittal, J. Song, S. Gupta, and T. A. Wettergren, "Rapid path planning for Dubins vehicles under environmental currents," *Robot. Auton. Syst.*, vol. 134, p. 103646, 2020.
- [40] K. Mittal and S. Gupta, "Minimum-time motion-planning of auvs under spatially varying ocean currents," in *Proceedings of IEEE/MTS OCEANS 2019*, Seattle, WA, USA, 2019.
- [41] R. Raval and S. Gupta, "Smart-oc: A real-time time-risk optimal replanning algorithm for dynamic obstacles and spatio-temporally varying currents," 2025. [Online]. Available: <https://arxiv.org/abs/2508.09508>
- [42] J. Song, S. Gupta, and T. A. Wettergren, "T*: Time-optimal risk-aware motion planning for curvature-constrained vehicles," *IEEE Robot. Automat. Lett.*, vol. 4, no. 1, pp. 33–40, 2019.
- [43] S. Karaman and E. Frazzoli, "Incremental sampling-based algorithms for optimal motion planning," *Robotics Science and Systems VI*, vol. 104, no. 2, pp. 267–274, 2010.
- [44] J. P. Wilson, S. Gupta, and T. A. Wettergren, "Generalized multispeed dubins motion model," *IEEE Transactions on Robotics*, vol. 41, pp. 2861–2878, 2025.
- [45] J. Song and S. Gupta, "CARE: Cooperative autonomy for resilience and efficiency of robot teams for complete coverage of unknown environments under robot failures," *Auton. Robots*, vol. 44, pp. 647–671, 2020.